In vivo retinal imaging by optical coherence tomography

E. A. Swanson

Lincoln Laboratory, Massachusetts Institute of Technology, 244 Wood Street, Lexington, Massachusetts 02173-9108

J. A. Izatt, M. R. Hee, and D. Huang

Department of Electrical Engineering and Computer Science, Massachusetts Institute of Technology, Cambridge, Massachusetts 02139

C. P. Lin, J. S. Schuman, and C. A. Puliafito

Laser Research Laboratory, New England Eye Center, Tufts University School of Medicine, Boston, Massachusetts 02111

J. G. Fujimoto

Department of Electrical Engineering and Computer Science, Massachusetts Institute of Technology, Cambridge, Massachusetts 02139

Received May 27, 1993

We describe what are to our knowledge the first *in vivo* measurements of human retinal structure with optical coherence tomography. These images represent the highest depth resolution *in vivo* retinal images to date. The tomographic system, image-processing techniques, and examples of high-resolution tomographs and their clinical relevance are discussed.

A number of promising new techniques have been developed for micrometer-resolution imaging of biological microstructure based on optical coherence domain reflectometry (OCDR). OCDR was originally demonstrated for applications in fiber-optic and integrated-optic structures[1–3] and has recently been applied to measurements in biological systems, including the eye[4–7] and artery.[8,9] We have recently described a new technique for two- or three-dimensional coherent imaging of biological structure called optical coherence tomography[10] (OCT). OCT is a noninvasive, noncontact tomographic imaging technique with superior spatial resolution to ultrasound (<20 μm) and high sensitivity (>100-dB dynamic range). OCT is particularly attractive in ophthalmic application, where it may potentially provide for quantitative diagnosis of a variety of ocular diseases. We have previously obtained OCT images in the anterior segment, crystalline lens, and retina of human eyes *in vitro*[10,11] and *in vivo*.[11] In this Letter we report the development and demonstration of what is to our knowledge the first high-speed micrometer-resolution OCT system for automated *in vivo* transpupillary measurements of the human retina.

Figure 1 shows the schematic of our system. The principle behind OCDR is well known and is not reviewed here.[1–9] The superluminescent diode source operated at ~843 nm, and the signal power delivered onto the patient eye was ~175 μW. This is in compliance with a conservative interpretation of the American National Standards Institute safe ocular exposure standard (ANSI Z136).[12] The FWHM spectral bandwidth of the source was ~30 nm, and the longitudinal FWHM resolution was measured at ~14 μm—near-transform-limited resolution.[7] The system longitudinal scanning speed was 160 mm/s, four times higher than previously reported results. This increase in speed greatly facilitates measurements on human subjects. Approximately 94 dB of dynamic range is obtained at a scan speed of 156 mm/s, near the quantum limit.[9]

In order to perform precise two-dimensional imaging of the retina, we have incorporated beam-steering devices and imaging optics onto a standard ophthalmic slit-lamp biomicroscope. Figure 2 shows a simplified optical schematic of the modified slit-lamp biomicroscope. The sample arm fiber output

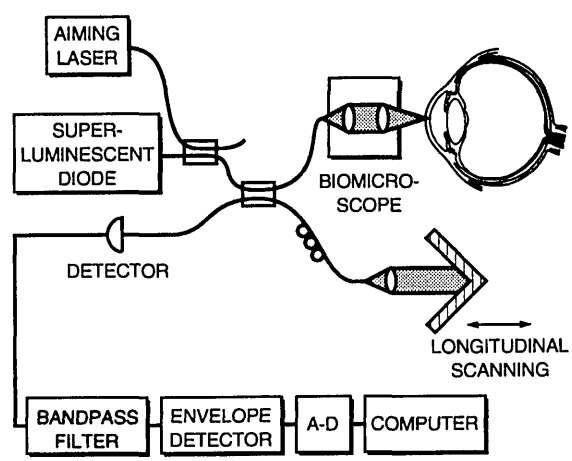

Fig. 1. Schematic of high-speed OCDR system. The system consists of a fiber-optic Michelson interferometer with a superluminescent diode source. High scanning speed is achieved by use of a fast slewing reference mirror. The optical ranging signal is derived by demodulation of the interferometer output at the Doppler frequency. A-D, analog-to-digital converter.

0146-9592/93/211864-03$6.00/0

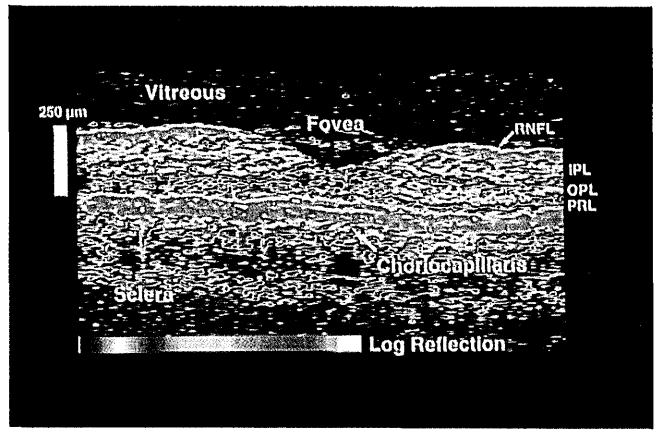

Plate I. Optical coherence tomograph of human retina in the macular region *in vivo*. Identifiable structure includes the vitreous region, retina, retinal nerve fiber layer (RNFL), fovea, choriocapillaris, inner and outer plexiform layers (IPL, OPL), photoreceptor layer (RPL), and sclera.

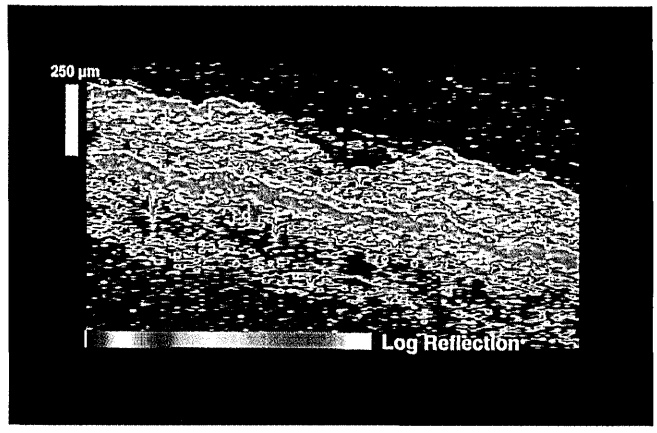

Plate II. Unprocessed image corresponding to Plate I.

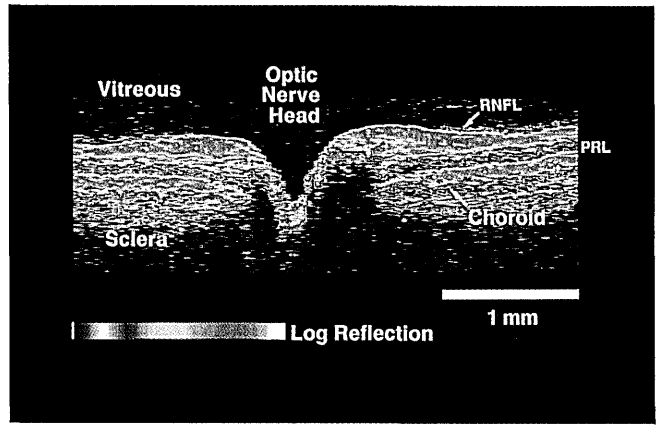

Plate III. *In vivo* optical coherence tomograph of the optic nerve head taken perpendicular to the papillomacular axis. Identifiable structures include retinal nerve fiber layer (RNFL), choroid, and optic disk profile.

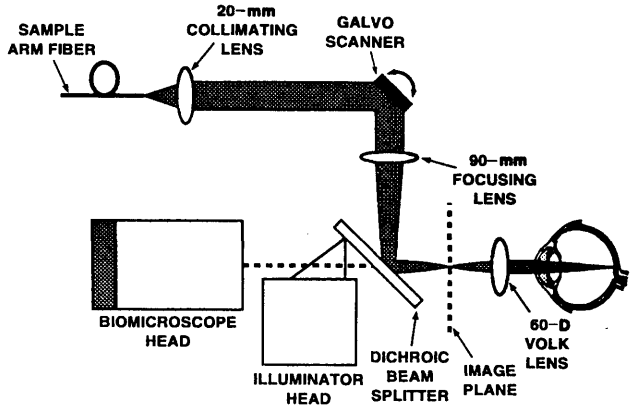

Fig. 2. Schematic of modified slit-lamp biomicroscope. The dichroic mirror combines OCT and the microscope path. Two galvanometric beam-steering devices provide lateral scan (only one axis is shown for simplicity). The 90-mm focusing lens, in combination with the 60-D Volk lens, is designed so as to image the scanning pupil at the patient pupil to eliminate beam shear.

is collimated with a 20-mm multielement collimating lens. The collimated superluminescent diode light is directed onto two orthogonally mounted computer-controlled galvanometric beam-steering devices. A dichroic beam splitter and a 90-mm focusing lens focuses and directs the light into the image plane of the slit lamp. A 60-D Volk lens, in combination with the patient eye optics, relays the image plane of the slit lamp onto the retina. The Volk lens is properly metered to relay the pupil of the superluminescent diode path (i.e., the face of the galvanometers) onto the entrance pupil of the eye, thereby minimizing vignetting. Computer control and data acquisition permit arbitrary scanning patterns on the retina and provide a real-time image of the scan in progress on a computer monitor. A 635-nm diode laser (Fig. 1) enables the operator to pinpoint where measurements are made.

Fast image acquisition time is important for high-resolution *in vivo* measurements since it minimizes motion induced artifacts. The image acquisition time is given by

$$T_{\mathrm{acq}} = \epsilon \frac{\text{scan depth}}{\text{scan velocity}} \text{no. transverse pixels},$$

where ϵ is an efficiency factor related to the duty cycle of the longitudinal scanning mechanism ($\epsilon \sim 1.125$). Subsequent tomographs were obtained with a scan depth of 3 mm, a scan velocity of 156 mm/s, and 100 transverse pixels, yielding an acquisition time of ~2.4 s. Subsecond acquisition times may be achieved by reduction of the number of transverse pixels and/or a further increase in the scan speed.

One important potential application of OCT is in noninvasive cross-sectional imaging of the retina. Optical imaging of the retina is challenging because the retina has structure on the micrometer scale, has weak backscattering, and is located at the back of the eye. Since the depth resolution of OCT is governed by the coherence properties of the light source, high-sensitivity micrometer-resolution imaging is possible at an arbitrary working distance. This is in contrast to scanning confocal retinal imaging systems such as scanning laser ophthalmology and scanning laser tomography, in which the pupil aperture and ocular aberrations limit the axial resolution to several hundred micrometers.[13,14]

Plate I shows a cross-sectional OCT image obtained in the macular region of a human volunteer. The fovea (the region of highest visual acuity) is visible as a characteristic thinning of the retina because of the lateral displacement of the photoreceptor cell synapses and the inner retinal neurons in the area of central vision. Laterally to the fovea, layers of high and low scattering reveal the stratified cellular structure of the retina. The retinal nerve fiber layer (RNFL), consisting of horizontal nerve fibers, is observed as a region of enhanced scattering near the vitreo–retinal interface. Also visible are stratifications indicative of the inner and outer plexiform layers and a dark layer that is indicative of low scattering within the photoreceptor layer. The highest scattering is visible from the choriocapillaris, which consists of a dense interconnected network of small blood vessels. To our knowledge, these retinal OCT images are the highest-resolution tomographic images of the living retina that have ever been obtained.

The retinal image in Plate I has been processed to remove artifacts that are due to patient motion. The raw data from Plate I are shown in Plate II. Motion artifacts show up as pixel-to-pixel jaggedness in the vitreo–retinal boundary as well as in larger-scale variations in the retinal surface position. An estimate of this motion is obtained with a cross-correlation technique in which the longitudinal index is chosen as the location of the peak correlation of adjacent scans. Figure 3 shows the estimated motion that occurred while the image of Plate I was acquired. As illustrated in Plate II, the peak index can be filtered to retain only selected spatial frequencies. In using this image-processing technique we find that there is a trade-off between correcting for motion artifacts and processing out real spatial variations within the structure itself. In the foveal region, where the macula is flat, we have selected a spatial cutoff frequency of 0 cycles/image.

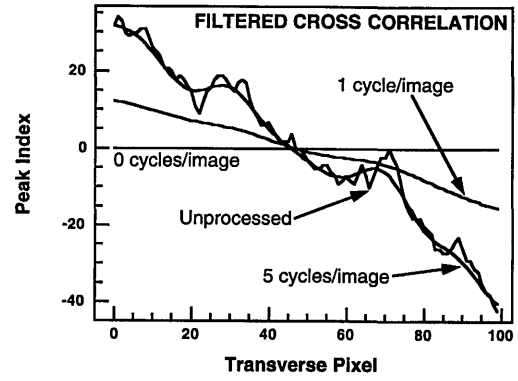

Fig. 3. Result of cross correlating adjacent scans to form an estimate of the motion-induced artifacts during the image acquisition of Plate II. Also shown is the result of spatially filtering motion to form estimates of the selective frequencies.

Plate III is a processed cross-sectional *in vivo* image through the optic nerve head taken perpendicular to the papillomacular axis. Enhanced scattering is again visible from the RNFL, which expands to occupy nearly the entire retinal thickness as a result of bundling of the nerve fibers as they enter the optic disk. The surface contour and cupping of the optic disk is well visualized. The termination of the choroid at the lamina cribrosa provides a clear landmark by which to make measurements of retinal and RNFL thicknesses at the nerve head margin and at reproducible distances from it. Plate III was processed with a spatial frequency cutoff of 10 cycles/image.

The capability of OCT for direct micrometer-resolution imaging of the retina shows significant promise for the diagnosis and quantitative monitoring of a variety of retinal diseases, including macular degeneration, macular hole, and macular edema. Accurate measurements of retinal and RNFL thicknesses are also relevant to glaucoma, for which conventional diagnosis is complicated by the fact that intraocular pressure measurements do not reliably predict disease progression, and measurable visual field loss and/or cupping of the optic disk may be detectable only after significant (as much as 50%) RNFL loss.[15,16] The unique facility that OCT provides for objective, direct measurements of RNFL thickness could thus be of significant benefit for early diagnosis and treatment.

In summary, we have demonstrated optical coherence tomography as a new diagnostic technique for performing noncontact, noninvasive, micrometer-resolution cross-sectional imaging of retinal structure. Recent improvements to our system permit image acquisition in live patients in less than 3 s, including real-time image updating on a computer monitor. We believe that OCT is thus a promising, clinically feasible technique for a variety of retinal imaging applications.

This research was supported in part by the U.S. Department of the Air Force, by National Institutes of Health grant RO1-GM35459-08, and by U.S. Office of Naval Research MFEL Program N00014-91-C-0084.

References

1. R. C. Youngquist, S. Carr, and D. E. N. Davies, Opt. Lett. **12,** 158 (1987).
2. K. Takada, I. Yokohama, K. Chida, and J. Noda, Appl. Opt. **26,** 1063 (1987).
3. H. H. Gilgen, R. P. Novak, R. P. Salathé, W. Hodel, and P. Beaud, J. Lightwave Technol. **7,** 1225 (1989).
4. A. F. Fercher, K. Mengedoht, and W. Werner, Opt. Lett. **13,** 186 (1988).
5. C. K. Hitzenberger, W. Drexler, C. Dolezal, F. Skorpik, M. Juchem, A. F. Fercher, and H. D. Gnad, Invest. Ophthalmol. Vis. Sci. **33,** 1886 (1993).
6. D. Huang, J. Wang, C. P. Lin, C. A. Puliafito, and J. G. Fujimoto, Lasers Surg. Med. **11,** 419 (1991).
7. E. A. Swanson, D. Huang, M. R. Hee, J. G. Fujimoto, C. P. Lin, and C. A. Puliafito, Opt. Lett. **17,** 151 (1992).
8. M. R. Hee, D. Huang, E. A. Swanson, and J. G. Fujimoto, J. Opt. Soc. Am. B **9,** 903 (1992).
9. X. Clivaz, F. Marquis-Weible, R. P. Salathé, R. P. Novak, and H. H. Gilgen, Opt. Lett. **17,** 4 (1992).
10. D. Huang, E. A. Swanson, C. P. Lin, J. S. Schuman, W. G. Stinson, W. Chang, M. R. Hee, T. Flotte, K. Gregory, C. A. Puliafito, and J. G. Fujimoto, Science **254,** 1178 (1991).
11. J. A. Izatt, M. R. Hee, D. Huang, J. G. Fujimoto, E. A. Swanson, C. P. Lin, J. S. Schuman, and C. A. Puliafito, Proc. Soc. Photo-Opt. Instrum. Eng. **1877,** 136 (1993).
12. The ocular safe exposure standard for permanent intrabeam viewing of 830-nm light assuming no scanning and a full 7-mm pupil aperture is 200 μW (ANSI Z136; American National Standards Institute, 1986).
13. R. H. Webb, G. W. Hughes, and F. C. Delori, Appl. Opt. **26,** 1492 (1987).
14. J. F. Bille, A. W. Dreher, and G. Zinser, in *Noninvasive Diagnostic Techniques in Ophthalmology,* S. J. Masters, ed. (Springer-Verlag, New York, 1990), p. 528.
15. A. Sommer, Am. J. Ophthalmol. **180,** 485 (1989).
16. H. A. Quigley and E. M. Addicks, Arch. Ophthalmol. **100,** 807 (1982).